Available online at www.sciencedirect.com
ScienceDirect
Computers and Mathematics with Applications 53 (2007) 1538–1560
An International Journal
computers & mathematics
with applications
www.elsevier.com/locate/camwa

Vibration analysis of spherical structural elements using the GDQ method

Francesco Tornabene, Erasmo Viola*

DISTART - Department, Faculty of Engineering, University of Bologna, Italy

Received 28 March 2006; accepted 31 March 2006

Abstract

This paper deals with the dynamical behaviour of hemispherical domes and spherical shell panels. The First-order Shear Deformation Theory (FSDT) is used to analyze the above moderately thick structural elements. The treatment is conducted within the theory of linear elasticity, when the material behaviour is assumed to be homogeneous and isotropic. The governing equations of motion, written in terms of internal resultants, are expressed as functions of five kinematic parameters, by using the constitutive and the congruence relationships. The boundary conditions considered are clamped (C), simply supported (S) and free (F) edge. Numerical solutions have been computed by means of the technique known as the Generalized Differential Quadrature (GDQ) Method. These results, which are based upon the FSDT, are compared with the ones obtained using commercial programs such as Abaqus, Ansys, Femap/Nastran, Straus, Pro/Engineer, which also elaborate a three-dimensional analysis. The effect of different grid point distributions on the convergence, the stability and the accuracy of the GDQ procedure is investigated. The convergence rate of the natural frequencies is shown to be fast and the stability of the numerical methodology is very good. The accuracy of the method is sensitive to the number of sampling points used, to their distribution and to the boundary conditions.

Keywords: Differential quadrature; GDQ method; Sampling point distribution; Free vibrations; Spherical shell panels

1. Introduction

Structures of shell revolution type have been widely used in many fields of engineering, where they give rise to optimum conditions for dynamical behaviour, strength and stability. Pressure vessels, cooling towers, water tanks, dome-shaped structures, dams, turbine engine components and so forth, perform particular functions over different branches of structural engineering.

The purpose of this paper is to study the dynamic behaviour of structures derived from shells of revolution. The equations given here incorporate the effects of transverse shear deformation and rotary inertia.

The geometric model refers to a moderately thick shell. The analysis will be performed by following two different investigations. In the first one, the solution is obtained by using the numerical technique termed GDQ method, which

* Corresponding author. Tel.: +39 051 209 3510; fax: +39 051 209 3495.
E-mail address: erasmo.viola@mail.ing.unibo.it (E. Viola).

0898-1221/$ - see front matter © 2007 Elsevier Ltd. All rights reserved.
doi:10.1016/j.camwa.2006.03.039

leads to a generalized eigenvalue problem. The main features of the numerical technique under discussion, as well as its historical development, are illustrated in Section 3.

The solution is given in terms of generalized displacement components of the points lying on the middle surface of the shell. At the moment it can only be pointed out that by using the GDQ technique the numerical statement of the problem does not pass through any variational formulation, but deals directly with the governing equations of motion.

Numerical results will also be computed by using commercial programs, which also elaborate three-dimensional analyses.

It should be noted that there are various two-dimensional theories of thin shells. Any two-dimensional theory of shells is an approximation of the real three-dimensional problem. Starting from Love's theory about the thin shells, which dates back to 100 years ago, a lot of contributions on this topic have been made since then. The main purpose has been that of seeking better and better approximations for the exact three-dimensional elasticity solutions for shells.

In the last fifty years refined two-dimensional linear theories of thin shells have been developed including important contributions by Sanders [1], Flügge [2], Niordson [3]. In these refined shell theories the deformation is based on the Kirchhoff–Love assumption. In other words, this theory assumes that normals to the shell middle-surface remain normal to it during deformations and unstretched in length.

It is worth noting that when the refined theories of thin shells are applied to thick shells, the errors could be quite large. With the increasing use of thick shells in various engineering applications, simple and accurate theories for thick shells have been developed. With respect to the thin shells, the thick shell theories take the transverse shear deformation and rotary inertia into account. The transverse shear deformation has been incorporated into shell theories by following the work of Reissner [4] for the plate theory.

Several studies have been presented earlier for the vibration analysis of such revolution shells and the most popular numerical tool in carrying out these analyses is currently the finite element method. The generalized collocation method based on the ring element method has also been applied [5,6]. With regard to the latter method each static and kinematic variable is transformed into a theoretically infinite Fourier series of harmonic components, with respect to the circumferential coordinates.

In this paper, the governing equations of motion are a set of five two-dimensional partial differential equations with variable coefficients. These fundamental equations are expressed in terms of kinematic parameters and can be obtained by combining the three basic sets of equations, namely balance, congruence and constitutive equations.

Referring to the formulation of the dynamic equilibrium in terms of harmonic amplitudes of mid-surface displacements and rotations, in this paper the system of second-order linear partial differential equations is solved, without resorting to the one-dimensional formulation of the dynamic equilibrium of the shell. Now, the discretization of the system leads to a standard linear eigenvalue problem, where two independent variables are involved.

In this way it is possible to compute the complete assessment of the modal shapes corresponding to natural frequencies of structures.

2. Basic governing equations

2.1. Shell geometry and kinematic equations

The geometry of the shell considered hereafter is a surface of revolution with a circular curved meridian. The notation for the coordinates is shown in Fig. 1. The total thickness of the shell is represented by h. The distance of each point from the shell mid-surface along the normal is ζ.

The coordinate along the meridional and circumferential directions are $\alpha_1 = \alpha_\varphi$ and $\alpha_2 = \alpha_\vartheta$, respectively. The distance of each point from the axis of revolution is $R_0(\varphi)$ and φ is the angle between the normal to the shell surface and the axis of revolution (Fig. 2).

The position of an arbitrary point within the shell material is known by the coordinates φ $(0 \leq \varphi \leq \pi)$, ϑ $(0 \leq \vartheta \leq 2\pi)$ upon the middle surface, and ζ directed along the outward normal and measured from the reference surface $(-h/2 \leq \zeta \leq h/2)$.

R_φ and R_ϑ are, in the general case, the radii of curvature in the meridional and circumferential directions. For a spherical surface R_φ and R_ϑ are constant and equal to the radius of the shell R.

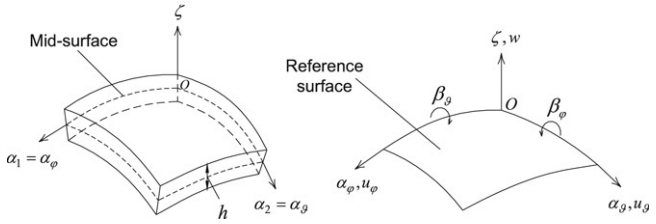

Fig. 1. Coordinate system of the shell and reference surface.

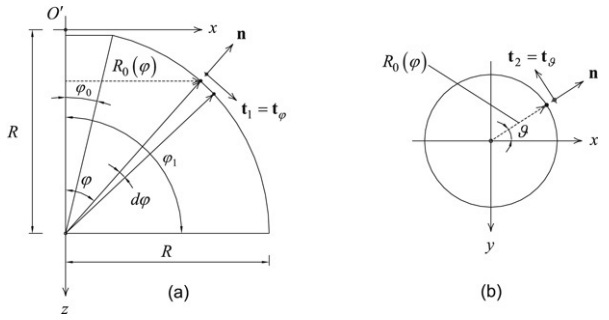

Fig. 2. Geometry of hemispherical dome.

The parametric coordinates (φ, ϑ) define, respectively, the meridional curves and the parallel circles upon the middle surface of the shell (Fig. 2). In developing a moderately thick shell theory we make certain assumptions. They are outlined below:

– The transverse normal is inextensible:

$$\varepsilon_n \approx 0.$$

– Normals to the reference surface of the shell before deformation remain straight but not necessarily normal after deformation (a relaxed Kirchhoff–Love hypothesis).

– The transverse normal stress is negligible so that the plane assumption can be invoked:

$$\sigma_n = \sigma_n(\alpha_1, \alpha_2, \zeta, t) = 0.$$

Consistent with the assumptions of a moderately thick shell theory, the displacement field assumed in this study is that of a *First-order Shear Deformation Theory* (FSDT) and can be put in the following form:

$$\begin{cases} U_\varphi(\alpha_\varphi, \alpha_\vartheta, \zeta, t) = u_\varphi(\alpha_\varphi, \alpha_\vartheta, t) + \zeta\beta_\varphi(\alpha_\varphi, \alpha_\vartheta, t) \\ U_\vartheta(\alpha_\varphi, \alpha_\vartheta, \zeta, t) = u_\vartheta(\alpha_\varphi, \alpha_\vartheta, t) + \zeta\beta_\vartheta(\alpha_\varphi, \alpha_\vartheta, t) \\ W(\alpha_\varphi, \alpha_\vartheta, \zeta, t) = w(\alpha_\varphi, \alpha_\vartheta, t) \end{cases} \tag{2.1}$$

where $u_\varphi, u_\vartheta, w$ are the displacement components of points lying on the middle surface ($\zeta = 0$) of the shell, along meridional, circumferential and normal directions, respectively. β_φ and β_ϑ are normals-to-mid-surface rotations, respectively.

The kinematics hypothesis expressed by Eq. (2.1) should be supplemented by the statement that the shell deflections are small and strains are infinitesimal, that is $w(\alpha_\varphi, \alpha_\vartheta, t) \ll h$.

It is worth noting that in-plane displacements U_φ and U_ϑ vary linearly through the thickness, while W remains independent of ζ. The relationships between strains and displacements along the shell reference (middle) surface

$\zeta = 0$ are the following:

$$\begin{aligned}
&\varepsilon_\varphi = \frac{1}{R}\left(\frac{\partial u_\varphi}{\partial \varphi} + w\right), \qquad \varepsilon_\vartheta = \frac{1}{R_0}\left(\frac{\partial u_\vartheta}{\partial \vartheta} + u_\varphi \cos\varphi + w \sin\varphi\right), \\
&\gamma_{\varphi\vartheta} = \frac{1}{R}\frac{\partial u_\vartheta}{\partial \varphi} + \frac{1}{R_0}\left(\frac{\partial u_\varphi}{\partial \vartheta} - u_\vartheta \cos\varphi\right) \\
&\kappa_\varphi = \frac{1}{R}\frac{\partial \beta_\varphi}{\partial \varphi}, \qquad \kappa_\vartheta = \frac{1}{R_0}\left(\frac{\partial \beta_\vartheta}{\partial \vartheta} + \beta_\varphi \cos\varphi\right), \qquad \kappa_{\varphi\vartheta} = \frac{1}{R}\frac{\partial \beta_\vartheta}{\partial \varphi} + \frac{1}{R_0}\left(\frac{\partial \beta_\varphi}{\partial \vartheta} - \beta_\vartheta \cos\varphi\right) \\
&\gamma_{\varphi n} = \frac{1}{R}\left(\frac{\partial w}{\partial \varphi} - u_\varphi\right) + \beta_\varphi, \qquad \gamma_{\vartheta n} = \frac{1}{R_0}\left(\frac{\partial w}{\partial \vartheta} - u_\vartheta \sin\varphi\right) + \beta_\vartheta
\end{aligned} \tag{2.2}$$

where $R_0(\varphi) = R \sin\varphi$ is the radius of a generic parallel of the spherical shell.

In the above, the first three strains $\varepsilon_\varphi, \varepsilon_\vartheta, \gamma_{\varphi\vartheta}$ are in-plane meridional, circumferential and shearing components, $\kappa_\varphi, \kappa_\vartheta, \kappa_{\varphi\vartheta}$ are the analogous curvature changes. The last two components are transverse shearing strains.

The matrix notation of the congruence equations assumes the aspect:

$$\boldsymbol{\varepsilon} = \mathbf{D}\mathbf{u} \tag{2.3}$$

where

$$\mathbf{D} = \begin{bmatrix}
\frac{1}{R}\frac{\partial}{\partial \varphi} & 0 & \frac{1}{R} & 0 & 0 \\
\frac{\cos\varphi}{R_0} & \frac{1}{R_0}\frac{\partial}{\partial \vartheta} & \frac{\sin\varphi}{R_0} & 0 & 0 \\
\frac{1}{R_0}\frac{\partial}{\partial \vartheta} & \frac{1}{R}\frac{\partial}{\partial \varphi} - \frac{\cos\varphi}{R_0} & 0 & 0 & 0 \\
0 & 0 & 0 & \frac{1}{R}\frac{\partial}{\partial \varphi} & 0 \\
0 & 0 & 0 & \frac{\cos\varphi}{R_0} & \frac{1}{R_0}\frac{\partial}{\partial \vartheta} \\
0 & 0 & 0 & \frac{1}{R_0}\frac{\partial}{\partial \vartheta} & \frac{1}{R}\frac{\partial}{\partial \varphi} - \frac{\cos\varphi}{R_0} \\
-\frac{1}{R} & 0 & \frac{1}{R}\frac{\partial}{\partial \varphi} & 1 & 0 \\
0 & -\frac{\sin\varphi}{R_0} & \frac{1}{R_0}\frac{\partial}{\partial \vartheta} & 0 & 1
\end{bmatrix} \tag{2.4}$$

is called the congruence operator or the kinematic operator and

$$\mathbf{u}(\alpha_\varphi, \alpha_\vartheta, t) = \begin{bmatrix} u_\varphi & u_\vartheta & w & \beta_\varphi & \beta_\vartheta \end{bmatrix}^{\mathrm{T}} \tag{2.5}$$

$$\boldsymbol{\varepsilon}(\alpha_\varphi, \alpha_\vartheta, t) = \begin{bmatrix} \varepsilon_\varphi & \varepsilon_\vartheta & \gamma_{\varphi\vartheta} & \kappa_\varphi & \kappa_\vartheta & \kappa_{\varphi\vartheta} & \gamma_{\varphi n} & \gamma_{\vartheta n} \end{bmatrix}^{\mathrm{T}} \tag{2.6}$$

denote the displacement vector and the generalized strain vector, respectively. The congruence operator is also known as the definition operator, because the Eq. (2.2) in discussion are known as the definition equations too.

2.2. Constitutive equations

The shell material assumed in the following is a mono-laminar elastic isotropic one. Accordingly, the following constitutive equations relate internal stress resultants and internal couples with generalized strain components on the middle surface:

$$
\begin{aligned}
&N_\varphi = K(\varepsilon_\varphi + \nu\varepsilon_\vartheta), \qquad M_\varphi = D(\kappa_\varphi + \nu\kappa_\vartheta), \qquad Q_\varphi = K\frac{(1-\nu)}{2\chi}\gamma_{\varphi n}\\
&N_\vartheta = K(\varepsilon_\vartheta + \nu\varepsilon_\varphi), \qquad M_\vartheta = D(\kappa_\vartheta + \nu\kappa_\varphi), \qquad Q_\vartheta = K\frac{(1-\nu)}{2\chi}\gamma_{\vartheta n}\\
&N_{\varphi\vartheta} = N_{\vartheta\varphi} = K\frac{(1-\nu)}{2}\gamma_{\varphi\vartheta}, \qquad M_{\varphi\vartheta} = M_{\vartheta\varphi} = D\frac{(1-\nu)}{2}\kappa_{\varphi\vartheta}
\end{aligned}
\tag{2.7}
$$

where $K = Eh/(1-\nu^2)$, $D = Eh^3/(12(1-\nu^2))$ are the membrane and bending rigidity, respectively. E is the Young modulus, ν is the Poisson ratio and χ is the shear factor which for isotropic materials is usually taken as $\chi = 6/5$. In Eq. (2.7), the first three components N_φ, N_ϑ, $N_{\varphi\vartheta}$ are the in-plane meridional, circumferential and shearing force resultants, M_φ, M_ϑ, $M_{\varphi\vartheta}$ are the analogous couples, while the last two Q_φ, Q_ϑ are the transverse shears.

In matrix notation, the relation between the generalized stress resultants per unit length and the generalized strain components takes the form:

$$
\mathbf{S} = \mathbf{C}\boldsymbol{\varepsilon} \tag{2.8}
$$

where

$$
\mathbf{C} = \begin{bmatrix}
K & \nu K & 0 & 0 & 0 & 0 & 0 & 0\\
\nu K & K & 0 & 0 & 0 & 0 & 0 & 0\\
0 & 0 & K\dfrac{1-\nu}{2} & 0 & 0 & 0 & 0 & 0\\
0 & 0 & 0 & D & \nu D & 0 & 0 & 0\\
0 & 0 & 0 & \nu D & D & 0 & 0 & 0\\
0 & 0 & 0 & 0 & 0 & D\dfrac{1-\nu}{2} & 0 & 0\\
0 & 0 & 0 & 0 & 0 & 0 & K\dfrac{1-\nu}{2\chi} & 0\\
0 & 0 & 0 & 0 & 0 & 0 & 0 & K\dfrac{1-\nu}{2\chi}
\end{bmatrix}
\tag{2.9}
$$

is the constitutive operator, also called matrix of the material rigidity and

$$
\mathbf{S}(\alpha_\varphi, \alpha_\vartheta, t) = \begin{bmatrix} N_\varphi & N_\vartheta & N_{\varphi\vartheta} & M_\varphi & M_\vartheta & M_{\varphi\vartheta} & Q_\varphi & Q_\vartheta \end{bmatrix}^{\mathrm{T}} \tag{2.10}
$$

is the vector of internal stress resultants also termed internal force vector.

2.3. Equations of motion in terms of internal actions

Following the direct approach or the Hamilton's principle in dynamic version and remembering the Gauss–Codazzi relations for the shells of revolution $\mathrm{d}R_0/\mathrm{d}\varphi = R_\varphi\cos\varphi = R\cos\varphi$, five equations of dynamic equilibrium in terms of internal actions can be written for the shell element:

$$
\begin{aligned}
&\frac{1}{R}\frac{\partial N_\varphi}{\partial\varphi} + \frac{1}{R_0}\frac{\partial N_{\varphi\vartheta}}{\partial\vartheta} + \frac{\cos\varphi}{R_0}(N_\varphi - N_\vartheta) + \frac{Q_\varphi}{R} + q_\varphi = I_0\ddot{u}_\varphi + I_1\ddot{\beta}_\varphi\\
&\frac{1}{R}\frac{\partial N_{\varphi\vartheta}}{\partial\varphi} + \frac{1}{R_0}\frac{\partial N_\vartheta}{\partial\vartheta} + 2\frac{\cos\varphi}{R_0}N_{\varphi\vartheta} + \frac{\sin\varphi}{R_0}Q_\vartheta + q_\vartheta = I_0\ddot{u}_\vartheta + I_1\ddot{\beta}_\vartheta\\
&\frac{1}{R}\frac{\partial Q_\varphi}{\partial\varphi} + \frac{1}{R_0}\frac{\partial Q_\vartheta}{\partial\vartheta} + \frac{\cos\varphi}{R_0}Q_\varphi - \frac{N_\varphi}{R} - \frac{\sin\varphi}{R_0}N_\vartheta + q_n = I_0\ddot{w}\\
&\frac{1}{R}\frac{\partial M_\varphi}{\partial\varphi} + \frac{1}{R_0}\frac{\partial M_{\varphi\vartheta}}{\partial\vartheta} + \frac{\cos\varphi}{R_0}(M_\varphi - M_\vartheta) - Q_\varphi + m_\varphi = I_1\ddot{u}_\varphi + I_2\ddot{\beta}_\varphi\\
&\frac{1}{R}\frac{\partial M_{\varphi\vartheta}}{\partial\varphi} + \frac{1}{R_0}\frac{\partial M_\vartheta}{\partial\vartheta} + 2\frac{\cos\varphi}{R_0}M_{\varphi\vartheta} - Q_\vartheta + m_\vartheta = I_1\ddot{u}_\vartheta + I_2\ddot{\beta}_\vartheta
\end{aligned}
\tag{2.11}
$$

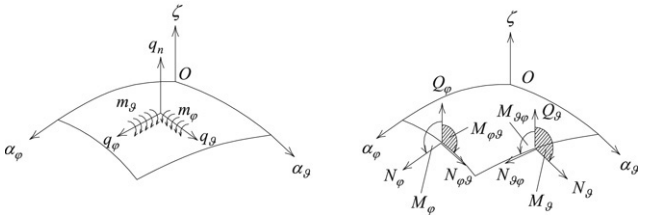

Fig. 3. Distributed external loads and generalized stress resultants.

where

$$I_0 = \mu h\left(1 + \frac{h^2}{12R^2}\right), \qquad I_1 = \frac{\mu h^3}{6R}, \qquad I_2 = \mu h^3\left(\frac{1}{12} + \frac{h^2}{80R^2}\right) \tag{2.12}$$

are the mass inertias and μ is the mass density of the material per unit volume. The first three Eq. (2.11) represent translational equilibriums along meridional, circumferential and normal directions, while the last two are rotational equilibrium equations about the φ and ϑ directions. Positive sign conventions for external loads per unit area as well as for stress resultants and couples are illustrated in Fig. 3.

Equations of motion or dynamic equilibrium equations (2.11) can be written in the operatorial form:

$$\mathbf{D}^*\mathbf{S} = \mathbf{q} - \frac{\partial \mathbf{\Lambda}}{\partial t} \qquad \text{or} \qquad \mathbf{D}^*\mathbf{S} = \mathbf{f} \tag{2.13}$$

where

$$\mathbf{q}(\alpha_\varphi, \alpha_\vartheta, t) = \begin{bmatrix} q_\varphi & q_\vartheta & q_n & m_\varphi & m_\vartheta \end{bmatrix}^{\mathrm{T}} \tag{2.14}$$

$$\mathbf{\Lambda}(\alpha_\varphi, \alpha_\vartheta, t) = \mathbf{M}\dot{\mathbf{u}} \tag{2.15}$$

are the distributed external load and the momentum vectors, respectively, and

$$\mathbf{M} = \begin{bmatrix} I_0 & 0 & 0 & I_1 & 0 \\ 0 & I_0 & 0 & 0 & I_1 \\ 0 & 0 & I_0 & 0 & 0 \\ I_1 & 0 & 0 & I_2 & 0 \\ 0 & I_1 & 0 & 0 & I_2 \end{bmatrix} \tag{2.16}$$

is the mass matrix, while

$$\dot{\mathbf{u}}(\alpha_\varphi, \alpha_\vartheta, t) = \frac{\partial}{\partial t}\begin{bmatrix} u_\varphi & u_\vartheta & w & \beta_\varphi & \beta_\vartheta \end{bmatrix}^{\mathrm{T}} \tag{2.17}$$

is the derivative of the displacement vector with respect to the variable t, that is the vector velocity.

The balance operator, also known as the equilibrium operator, assumes the aspect:

$$\mathbf{D}^* = -\begin{bmatrix} \frac{\cos\varphi}{R_0} + \frac{1}{R}\frac{\partial}{\partial\varphi} & -\frac{\cos\varphi}{R_0} & \frac{1}{R_0}\frac{\partial}{\partial\vartheta} & 0 & 0 & 0 & \frac{1}{R} & 0 \\ 0 & \frac{1}{R_0}\frac{\partial}{\partial\vartheta} & 2\frac{\cos\varphi}{R_0} + \frac{1}{R}\frac{\partial}{\partial\varphi} & 0 & 0 & 0 & 0 & \frac{\sin\varphi}{R_0} \\ -\frac{1}{R} & -\frac{\sin\varphi}{R_0} & 0 & 0 & 0 & 0 & \frac{\cos\varphi}{R_0} + \frac{1}{R}\frac{\partial}{\partial\varphi} & \frac{1}{R_0}\frac{\partial}{\partial\vartheta} \\ 0 & 0 & 0 & \frac{\cos\varphi}{R_0} + \frac{1}{R}\frac{\partial}{\partial\varphi} & -\frac{\cos\varphi}{R_0} & \frac{1}{R_0}\frac{\partial}{\partial\vartheta} & -1 & 0 \\ 0 & 0 & 0 & 0 & \frac{1}{R_0}\frac{\partial}{\partial\vartheta} & 2\frac{\cos\varphi}{R_0} + \frac{1}{R}\frac{\partial}{\partial\varphi} & 0 & -1 \end{bmatrix}. \tag{2.18}$$

2.4. Fundamental equations

The three basic sets of equations, namely the kinematic, the equilibrium and the constitutive equations may be combined to give the fundamental system of equations, also known as the governing system equations. Firstly, the

fundamental equations are deduced in the matrix notation. So, if the strain–displacement relations (2.3) are inserted into the constitutive Eq. (2.8), we have the relationships between stress resultants and the generalized displacement components:

$$\mathbf{S} = \mathbf{C}\boldsymbol{\varepsilon} = \mathbf{CDu}. \tag{2.19}$$

When the Eq. (2.19) are inserted into the equations of motion (2.13), the fundamental system of equations is derived:

$$\mathbf{D}^*\mathbf{CDu} = \mathbf{q} - \frac{\partial \boldsymbol{\Lambda}}{\partial t} \quad \text{or} \quad \mathbf{D}^*\mathbf{CDu} = \mathbf{f}. \tag{2.20}$$

The equations of motion in terms of displacements take all the three aspects of the problem of the elastic equilibrium into account.

By introducing the fundamental operator, also known as the elasticity operator:

$$\mathbf{L} = \mathbf{D}^*\mathbf{CDu}. \tag{2.21}$$

Eq. (2.20) can be written as:

$$\mathbf{Lu} = \mathbf{q} - \frac{\partial \boldsymbol{\Lambda}}{\partial t} \quad \text{or} \quad \mathbf{Lu} = \mathbf{f}. \tag{2.22}$$

The fundamental system of Eq. (2.22) relates the configuration variable $\mathbf{u}$ to the source variable $\mathbf{q}$ of the phenomenon under investigation.

We can summarize all these aspects of any problem of elastic problem of equilibrium into the scheme of the physical theories or Tonti's diagram, which assumes the aspect reported in Fig. 4.

Substituting the definition equation (2.2) into the constitutive equation (2.7) and the result of this substitution into the equilibrium equation (2.11), the complete equations of motion in terms of displacements can be written in the extended form as:

$$\begin{aligned}
&\frac{K}{R^2}\frac{\partial^2 u_\varphi}{\partial \varphi^2} + \frac{(1-\nu)}{2}\frac{K}{R_0^2}\frac{\partial^2 u_\varphi}{\partial \vartheta^2} + \frac{(1+\nu)}{2}\frac{K}{RR_0}\frac{\partial^2 u_\vartheta}{\partial \varphi \partial \vartheta} + K\frac{\cos\varphi}{RR_0}\frac{\partial u_\varphi}{\partial \varphi} \\
&\quad + \frac{K}{R}\left[\frac{1}{R}\left(1 + \frac{(1-\nu)}{2\chi}\right) + \frac{\nu \sin\varphi}{R_0}\right]\frac{\partial w}{\partial \varphi} - K\frac{(3-\nu)}{2}\frac{\cos\varphi}{R_0^2}\frac{\partial u_\vartheta}{\partial \vartheta} \\
&\quad - K\left[\frac{1}{R_0}\left(\frac{\nu \sin\varphi}{R} + \frac{\cos^2\varphi}{R_0}\right) + \frac{1}{R^2}\frac{(1-\nu)}{2\chi}\right]u_\varphi + K\frac{\cos\varphi}{R_0}\left(\frac{1}{R} - \frac{\sin\varphi}{R_0}\right)w \\
&\quad + \frac{(1-\nu)}{2\chi}\frac{K}{R}\beta_\varphi + q_\varphi = \mu h\left(1 + \frac{h^2}{12R^2}\right)\ddot{u}_\varphi + \frac{\mu h^3}{6R}\ddot{\beta}_\varphi
\end{aligned} \tag{2.23}$$

$$\begin{aligned}
&\frac{(1-\nu)}{2}\frac{K}{R^2}\frac{\partial^2 u_\vartheta}{\partial \varphi^2} + \frac{K}{R_0^2}\frac{\partial^2 u_\vartheta}{\partial \vartheta^2} + \frac{(1+\nu)}{2}\frac{K}{RR_0}\frac{\partial^2 u_\varphi}{\partial \varphi \partial \vartheta} + K\frac{(1-\nu)}{2}\frac{\cos\varphi}{RR_0}\frac{\partial u_\vartheta}{\partial \varphi} \\
&\quad + K\frac{(3-\nu)}{2}\frac{\cos\varphi}{R_0^2}\frac{\partial u_\varphi}{\partial \vartheta} + \frac{K}{R_0}\left[\frac{\nu}{R} + \frac{\sin\varphi}{R_0}\left(1 + \frac{(1-\nu)}{2\chi}\right)\right]\frac{\partial w}{\partial \vartheta} \\
&\quad + \frac{(1-\nu)}{2}\frac{K}{R_0}\left[\frac{\sin\varphi}{R} - \frac{1}{R_0}\left(\cos^2\varphi + \frac{\sin^2\varphi}{\chi}\right)\right]u_\vartheta \\
&\quad + K\frac{(1-\nu)}{2\chi}\frac{\sin\varphi}{R_0}\beta_\vartheta + q_\vartheta = \mu h\left(1 + \frac{h^2}{12R^2}\right)\ddot{u}_\vartheta + \frac{\mu h^3}{6R}\ddot{\beta}_\vartheta
\end{aligned} \tag{2.24}$$

$$\begin{aligned}
&\frac{(1-\nu)}{2\chi}\frac{K}{R^2}\frac{\partial^2 w}{\partial \varphi^2} + \frac{(1-\nu)}{2\chi}\frac{K}{R_0^2}\frac{\partial^2 w}{\partial \vartheta^2} - \frac{K}{R}\left[\frac{1}{R}\left(1 + \frac{(1-\nu)}{2\chi}\right) + \frac{\nu \sin\varphi}{R_0}\right]\frac{\partial u_\varphi}{\partial \varphi} \\
&\quad + K\frac{(1-\nu)}{2\chi}\frac{\cos\varphi}{RR_0}\frac{\partial w}{\partial \varphi} + \frac{(1-\nu)}{2\chi}\frac{K}{R}\frac{\partial \beta_\varphi}{\partial \varphi} - \frac{K}{R_0}\left[\frac{\nu}{R} + \frac{\sin\varphi}{R_0}\left(1 + \frac{(1-\nu)}{2\chi}\right)\right]\frac{\partial u_\vartheta}{\partial \vartheta}
\end{aligned}$$

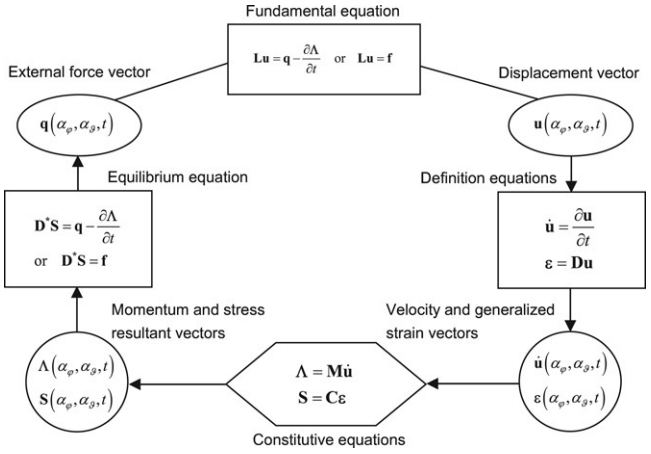

Fig. 4. The scheme of the physical theories or the Tonti's diagram.

$$+\frac{(1-\nu)}{2\chi}\frac{K}{R_0}\frac{\partial\beta_\vartheta}{\partial\vartheta}-K\frac{\cos\varphi}{R_0}\left[\frac{\sin\varphi}{R_0}+\frac{1}{R}\left(\nu+\frac{(1-\nu)}{2\chi}\right)\right]u_\varphi$$
$$-K\left[\frac{1}{R}\left(\frac{1}{R}+\frac{2\nu\sin\varphi}{R_0}\right)+\frac{\sin^2\varphi}{R_0^2}\right]w+K\frac{(1-\nu)}{2\chi}\frac{\cos\varphi}{R_0}\beta_\varphi+q_n=\mu h\left(1+\frac{h^2}{12R^2}\right)\ddot{w} \tag{2.25}$$

$$\frac{D}{R^2}\frac{\partial^2\beta_\varphi}{\partial\varphi^2}+\frac{(1-\nu)}{2}\frac{D}{R_0^2}\frac{\partial^2\beta_\varphi}{\partial\vartheta^2}+\frac{(1+\nu)}{2}\frac{D}{RR_0}\frac{\partial^2\beta_\vartheta}{\partial\varphi\partial\vartheta}-\frac{(1-\nu)}{2\chi}\frac{K}{R}\frac{\partial w}{\partial\varphi}$$
$$+D\frac{\cos\varphi}{RR_0}\frac{\partial\beta_\varphi}{\partial\varphi}-D\frac{(3-\nu)}{2}\frac{\cos\varphi}{R_0^2}\frac{\partial\beta_\vartheta}{\partial\vartheta}+\frac{(1-\nu)}{2\chi}\frac{K}{R}u_\varphi$$
$$-\left[\frac{D}{R_0}\left(\frac{\nu\sin\varphi}{R}+\frac{\cos^2\varphi}{R_0}\right)+K\frac{(1-\nu)}{2\chi}\right]\beta_\varphi+m_\varphi=\frac{\mu h^3}{6R}\ddot{u}_\varphi+\mu h^3\left(\frac{1}{12}+\frac{h^2}{80R^2}\right)\ddot{\beta}_\varphi \tag{2.26}$$

$$\frac{(1-\nu)}{2}\frac{D}{R^2}\frac{\partial^2\beta_\vartheta}{\partial\varphi^2}+\frac{D}{R_0^2}\frac{\partial^2\beta_\vartheta}{\partial\vartheta^2}+\frac{(1+\nu)}{2}\frac{D}{RR_0}\frac{\partial^2\beta_\varphi}{\partial\varphi\partial\vartheta}+D\frac{(1-\nu)}{2}\frac{\cos\varphi}{RR_0}\frac{\partial\beta_\vartheta}{\partial\varphi}$$
$$-\frac{(1-\nu)}{2\chi}\frac{K}{R_0}\frac{\partial w}{\partial\vartheta}+D\frac{(3-\nu)}{2}\frac{\cos\varphi}{R_0^2}\frac{\partial\beta_\varphi}{\partial\vartheta}+K\frac{(1-\nu)}{2\chi}\frac{\sin\varphi}{R_0}u_\vartheta$$
$$+\left[\frac{(1-\nu)}{2}\frac{D}{R_0}\left(\frac{\sin\varphi}{R}-\frac{\cos^2\varphi}{R_0}\right)-K\frac{(1-\nu)}{2\chi}\right]\beta_\vartheta+m_\vartheta=\frac{\mu h^3}{6R}\ddot{u}_\vartheta+\mu h^3\left(\frac{1}{12}+\frac{h^2}{80R^2}\right)\ddot{\beta}_\vartheta. \tag{2.27}$$

2.5. Boundary and compatibility conditions

In the following, three kinds of boundary conditions are considered, namely the fully clamped edge boundary conditions (C), the simply supported edge boundary conditions (S) and the free edge boundary conditions (F). The equations describing the boundary conditions can be written as follows:

Clamped edge boundary condition (C):

$$u_\varphi=u_\vartheta=w=\beta_\varphi=\beta_\vartheta=0\quad\text{at }\varphi=\varphi_0\text{ or }\varphi=\varphi_1,\ 0\le\vartheta\le\vartheta_0 \tag{2.28}$$
$$u_\varphi=u_\vartheta=w=\beta_\varphi=\beta_\vartheta=0\quad\text{at }\vartheta=0\text{ or }\vartheta=\vartheta_0,\ \varphi_0\le\varphi\le\varphi_1. \tag{2.29}$$

Simply supported edge boundary condition (S):

$$u_\varphi=u_\vartheta=w=\beta_\vartheta=0,\qquad M_\varphi=0\quad\text{at }\varphi=\varphi_0\text{ or }\varphi=\varphi_1,\ 0\le\vartheta\le\vartheta_0 \tag{2.30}$$
$$u_\varphi=u_\vartheta=w=\beta_\varphi=0,\qquad M_\vartheta=0\quad\text{at }\vartheta=0\text{ or }\vartheta=\vartheta_0,\ \varphi_0\le\varphi\le\varphi_1. \tag{2.31}$$

Free edge boundary condition (F):

$$N_\varphi = N_{\varphi\vartheta} = Q_\varphi = M_\varphi = M_{\varphi\vartheta} = 0 \quad \text{at } \varphi = \varphi_0 \text{ or } \varphi = \varphi_1,\ 0 \le \vartheta \le \vartheta_0 \tag{2.32}$$

$$N_\vartheta = N_{\varphi\vartheta} = Q_\vartheta = M_\vartheta = M_{\varphi\vartheta} = 0 \quad \text{at } \vartheta = 0 \text{ or } \vartheta = \vartheta_0,\ \varphi_0 \le \varphi \le \varphi_1. \tag{2.33}$$

In addition to the external boundary conditions, the *kinematical* and *physical compatibility* should be satisfied at the common meridian with $\vartheta = 0, 2\pi$, if we want to consider a complete hemispherical dome of revolution. The kinematical compatibility conditions include the continuity of displacements. The physical compatibility conditions can only be the five continuous conditions for the generalized stress resultants. To consider a complete revolute hemispherical dome characterized by $\vartheta_0 = 2\pi$, it is necessary to implement the kinematical and physical compatibility conditions between the meridians with $\vartheta = 0$ and with $\vartheta_0 = 2\pi$:

Kinematical compatibility conditions:

$$\begin{aligned} &u_\varphi(\varphi,0,t) = u_\varphi(\varphi,2\pi,t), \qquad u_\vartheta(\varphi,0,t) = u_\vartheta(\varphi,2\pi,t), \qquad w(\varphi,0,t) = w(\varphi,2\pi,t),\\ &\beta_\varphi(\varphi,0,t) = \beta_\varphi(\varphi,2\pi,t), \qquad \beta_\vartheta(\varphi,0,t) = \beta_\vartheta(\varphi,2\pi,t)\\ &\varphi_0 \le \varphi \le \varphi_1. \end{aligned} \tag{2.34}$$

Physical compatibility conditions:

$$\begin{aligned} &N_\vartheta(\varphi,0,t) = N_\vartheta(\varphi,2\pi,t), \qquad N_{\varphi\vartheta}(\varphi,0,t) = N_{\varphi\vartheta}(\varphi,2\pi,t), \qquad Q_\vartheta(\varphi,0,t) = Q_\vartheta(\varphi,2\pi,t),\\ &M_\vartheta(\varphi,0,t) = M_\vartheta(\varphi,2\pi,t), \qquad M_{\varphi\vartheta}(\varphi,0,t) = M_{\varphi\vartheta}(\varphi,2\pi,t)\\ &\varphi_0 \le \varphi \le \varphi_1. \end{aligned} \tag{2.35}$$

3. Generalized differential quadrature method

The GDQ method will be used to discretize the derivatives in the governing equations and the boundary conditions. The GDQ approach was developed by Shu [7] to improve the Differential Quadrature technique [8–11] for the computation of weighting coefficients, entering into the linear algebraic system of equations obtained from the discretization of the differential equation system, which can model the physical problem considered [12–16]. The essence of the differential quadrature method is that the partial derivative of a smooth function with respect to a variable is approximated by a weighted sum of function values at all discrete points in that direction. Its weighting coefficients are not related to any special problem and only depend on the grid points and the derivative order. In this methodology, an arbitrary grid distribution can be chosen without any limitation.

The GDQ method is based on the analysis of a high-order polynomial approximation and the analysis of a linear vector space [17]. For a general problem, it may not be possible to express the solution of the corresponding partial differential equation in a closed form. This solution function can be approximated by the two following types of function approximation: high-order polynomial approximation and Fourier series expansion (harmonic functions). It is well known that a smooth function in a domain can be accurately approximated by a high-order polynomial in accordance with the Weierstrass polynomial approximation theorem. In fact, from the Weierstrass theorem, if $f(x)$ is a real valued continuous function defined in the closed interval $[a, b]$, then there exists a sequence of polynomials $P_K(x)$ which converges to $f(x)$ uniformly as K goes to infinity. In practical applications, a truncated finite polynomial may be used. Thus, if $f(x)$ represents the solution of a partial differential equation, then it can be approximated by a polynomial of a degree less than or equal to $N-1$, for N large enough. The conventional form of this approximation is:

$$f(x) \cong P_N(x) = \sum_{j=1}^{N} d_j p_j(x) \tag{3.1}$$

where d_j is a constant. Then, it is easy to show that the polynomial $P_N(x)$ constitutes an N-dimensional linear vector space V_N with respect to the operation of vector addition and scalar multiplication. Obviously, in the linear vector space V_N, $p_j(x)$ is a set of base vectors. It can be seen that, in the linear polynomial vector space, there exist several sets of base polynomials and each set of base polynomials can be expressed uniquely by another set of base polynomials in the space. Using vector space analysis, the method for computing the weighting coefficients can be

generalized by a proper choice of base polynomials in a linear vector space. For generality, the Lagrange interpolation polynomials are chosen as the base polynomials. As a result, the weighting coefficients of the first-order derivative are computed by a simple algebraic formulation without any restriction on the choice of the grid points, while the weighting coefficients of the second- and higher-order derivatives are given by a recurrence relationship.

When the Lagrange interpolated polynomials are assumed as a set of vector space base functions, the approximation of the function $f(x)$ can be written as:

$$f(x) \cong \sum_{j=1}^{N} p_j(x) f(x_j) \tag{3.2}$$

where N is the number of grid points in the whole domain, x_j, $j = 1, 2, \ldots, N$, are the coordinates of grid points in the variable domain and $f(x_j)$ are the function values at the grid points. $p_j(x)$ are the Lagrange interpolated polynomials, which can be defined by the following formula:

$$p_j(x) = \frac{\mathbf{L}(x)}{(x - x_j)\mathbf{L}^{(1)}(x_j)}, \qquad j = 1, 2, \ldots, N \tag{3.3}$$

where:

$$\mathbf{L}(x) = \prod_{i=1}^{N}(x - x_i), \qquad \mathbf{L}^{(1)}(x_j) = \prod_{i=1, i\neq j}^{N}(x_j - x_i). \tag{3.4}$$

Differentiating Eq. (3.2) with respect to x and evaluating the first derivative at a certain point of the function domain, it is possible to obtain:

$$f^{(1)}(x_i) \cong \sum_{j=1}^{N} p_j^{(1)}(x_i) f(x_j) = \sum_{j=1}^{N} \varsigma_{ij}^{(1)} f(x_j), \quad i = 1, 2, \ldots, N \tag{3.5}$$

where $\varsigma_{ij}^{(1)}$ are the GDQ weighting coefficients of the first-order derivative and x_i denote the coordinates of the grid points. In particular, it is worth noting that the weighting coefficients of the first-order derivative can be computed as:

$$p_j^{(1)}(x_i) = \varsigma_{ij}^{(1)} = \frac{\mathbf{L}^{(1)}(x_i)}{(x_i - x_j)\mathbf{L}^{(1)}(x_j)}, \quad i, j = 1, 2, \ldots, N, i \neq j. \tag{3.6}$$

From Eq. (3.6), $\varsigma_{ij}^{(1)}$ $(i \neq j)$ can be easily computed. However, the calculation of $\varsigma_{ii}^{(1)}$ is not easy to compute. According to the analysis of a linear vector space, one set of base functions can be expressed uniquely by a linear sum of another set of base functions. Thus, if one set of base polynomials satisfy a linear equation like (3.5), so does another set of base polynomials. As a consequence, the equation system for determining $\varsigma_{ij}^{(1)}$ and derived from the Lagrange interpolation polynomials should be equivalent to that derived from another set of base polynomials, i.e. $p_j(x) = x^{j-1}$, $j = 1, 2, \ldots, N$. Thus, $\varsigma_{ij}^{(1)}$ satisfies the following equation, which is obtained by the base polynomials $p_j(x) = x^{j-1}$, when $j = 1$:

$$\sum_{j=1}^{N} \varsigma_{ij}^{(1)} = 0 \Rightarrow \varsigma_{ii}^{(1)} = -\sum_{j=1, j\neq i}^{N} \varsigma_{ij}^{(1)}, \quad i, j = 1, 2, \ldots, N. \tag{3.7}$$

Eqs. (3.6) and (3.7) are two formulations to compute the weighting coefficients $\varsigma_{ij}^{(1)}$. It should be noted that, in the development of these two formulations, two sets of base polynomials were used in the linear polynomial vector space V_N. Finally, the nth-order derivative of function $f(x)$ with respect to x at grid points x_i, can be approximated by the GDQ approach:

$$\left.\frac{\mathrm{d}^n f(x)}{\mathrm{d}x^n}\right|_{x=x_i} = \sum_{j=1}^{N} \varsigma_{ij}^{(n)} f(x_j), \quad i = 1, 2, \ldots, N \tag{3.8}$$

where $\varsigma_{ij}^{(n)}$ are the weighting coefficients of the nth-order derivative. Similar to the first-order derivative and according to the polynomial approximation and the analysis of a linear vector space, it is possible to determine a recurrence relationship to compute the second- and higher-order derivatives. Thus, the weighting coefficients can be generated by the following recurrent formulation:

$$\varsigma_{ij}^{(n)} = n\left(\varsigma_{ii}^{(n-1)}\varsigma_{ij}^{(1)} - \frac{\varsigma_{ij}^{(n-1)}}{x_i - x_j}\right), \quad i \neq j, n = 2, 3, \ldots, N-1, i, j = 1, 2, \ldots, N \tag{3.9}$$

$$\sum_{j=1}^{N} \varsigma_{ij}^{(n)} = 0 \Rightarrow \varsigma_{ii}^{(n)} = -\sum_{j=1, j\neq i}^{N} \varsigma_{ij}^{(n)}, \quad n = 2, 3, \ldots, N-1, i, j = 1, 2, \ldots, N. \tag{3.10}$$

It is obvious from the above equations that the weighting coefficients of the second- and higher-order derivatives can be determined from those of the first-order derivative. Furthermore, it is interesting to note that, the preceding coefficients $\varsigma_{ij}^{(n)}$ are dependent on the derivative order n, on the grid point distribution x_j, $j = 1, 2, \ldots, N$, and on the specific point x_i, where the derivative is computed. There is no need to obtain the weighting coefficients from a set of algebraic equations which could be ill-conditioned when the number of grid points is large. Furthermore, this set of expressions for the determination of the weighting coefficients is so compact and simple that it is very easy to implement them in formulating and programming, because of the recurrence feature.

3.1. Grid distributions

Another important point for successful application of the GDQ method is how to distribute the grid points. In fact, the accuracy of this method is usually sensitive to the grid point distribution. The optimal grid point distribution depends on the order of derivatives in the boundary condition and the number of grid points used. The grid point distribution also plays an essential role in determining the convergence speed and stability of the GDQ method. In this paper, the effects of the grid point distribution will be investigated for the vibration analysis of spherical shells. The natural and simplest choice of the grid points through the computational domain is the one having equally spaced points in the coordinate direction of the computational domain. However, it is demonstrated that non-uniform grid distribution usually yields better results than equally spaced distribution. Quan and Chang [10,11] compared numerically the performances of the often-used non-uniform meshes and concluded that the grid points originating from the Chebyshev polynomials of the first kind are optimum in all the cases examined there. The zeros of orthogonal polynomials are the rational basis for the grid points. Shu [7] has used other choice which has given better results than the zeros of Chebyshev and Legendre polynomials. Bert and Malik [18] indicated that the preferred type of grid points changes with problems of interest and recommended the use of Chebyshev–Gauss–Lobatto grid for the structural mechanics computation. With Lagrange interpolating polynomials, the Chebyshev–Gauss–Lobatto sampling point rule proves efficient for numerical reasons [19,20] so that for such a collocation the approximation error of the dependent variables decreases as the number of nodes increases.

In this study, different grid point distributions are considered to investigate their effect on the GDQ solution accuracy, convergence speed and stability. The typical distributions of grid points, which are commonly used in the literature, in normalized form are reported as follows:

Equally spaced or uniform distribution (Uni)

$$r_i = \frac{i-1}{N-1}, \quad i = 1, 2, \ldots, N. \tag{3.11}$$

Roots of Chebyshev polynomials of the first kind (C I°)

$$r_i = \frac{g_i - g_1}{g_N - g_1}, \qquad g_i = \cos\left(\left(\frac{2i-1}{2N}\right)\pi\right), \quad i = 1, 2, \ldots, N. \tag{3.12}$$

Roots of Chebyshev polynomials of the second kind (C II°)

$$r_i = \frac{g_i - g_1}{g_N - g_1}, \qquad g_i = \cos\left(\frac{i\pi}{N+1}\right), \quad i = 1, 2, \ldots, N. \tag{3.13}$$

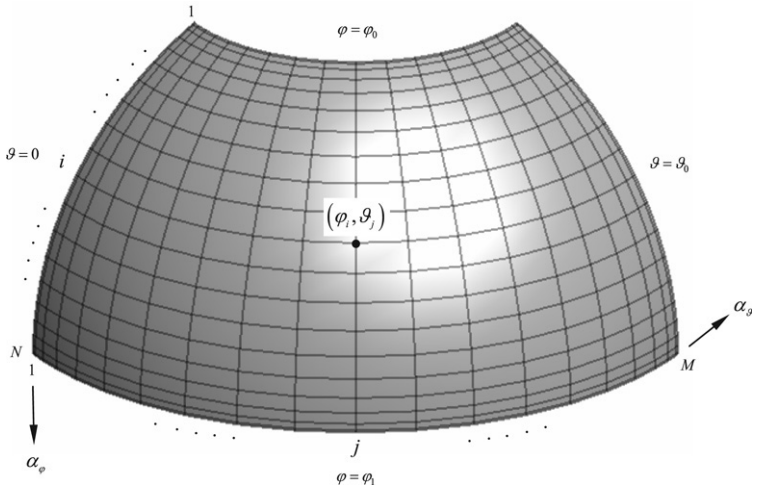

Fig. 5. C–G grid distribution on a hemispherical panel.

Roots of Legendre polynomials (Leg)

$$r_i = \frac{g_i - g_1}{g_N - g_1}, \qquad g_i = \left(1 - \frac{1}{8N^2} + \frac{1}{8N^3}\right)\cos\left(\frac{4i-1}{4N+2}\pi\right), \quad i = 1, 2, \ldots, N. \tag{3.14}$$

Quadratic sampling point distribution (Quad)

$$r_i = \begin{cases} 2\left(\dfrac{i-1}{N-1}\right)^2 & i = 1, 2, \ldots, \dfrac{N+1}{2} \\ \left(-2\left(\dfrac{i-1}{N-1}\right)^2 + 4\left(\dfrac{i-1}{N-1}\right) - 1\right) & i = \left(\dfrac{N+1}{2}\right) + 1, \ldots, N. \end{cases} \tag{3.15}$$

Chebyshev–Gauss–Lobatto sampling points (C–G)

$$r_i = \frac{1 - \cos(\frac{i-1}{N-1})\pi}{2}, \quad i = 1, 2, \ldots, N \tag{3.16}$$

where N is the total number of sampling points used to discretize each direction.

Apart the previous typical distributions, it is possible to stretch the traditional grid points towards the boundary using the *stretch formulation* [20]:

$$r_i = (1-\beta)(3l_i^3 - 2l_i^3) + \beta l_i, \quad i = 1, \ldots, N \tag{3.17}$$

where β is the stretching parameter and l_i are the coordinates of the typical grid point distributions reported above.

For the numerical computations presented in this paper, the coordinates of grid points (φ_i, ϑ_j) are chosen as:

$$\begin{aligned} &\varphi_i = r_i(\varphi_1 - \varphi_0) + \varphi_0, \quad i = 1, 2, \ldots, N, \text{ for } \varphi \in [\varphi_0, \varphi_1] \text{ (with } \varphi_0 > 0 \text{ and } \varphi_1 \le 90^\circ) \\ &\vartheta_j = r_j\vartheta_0, \quad j = 1, 2, \ldots, M, \text{ for } \vartheta \in [0, \vartheta_0] \text{ (with } \vartheta_0 \le 2\pi) \end{aligned} \tag{3.18}$$

where r_i, r_j are two grid distributions of previous ones and N, M are the total number of sampling points used to discretize the domain in φ and ϑ directions, respectively, of the spherical shell (Fig. 5).

4. Numerical implementation

A novel approach in numerically solving the governing Eqs. (2.23)–(2.27) is represented by the Generalized Differential Quadrature (GDQ) method. This method, for the problem studied herein, demonstrates its numerical accuracy and extreme coding simplicity.

In the following, only the free vibration of hemispherical dome or panel will be studied. So, setting $\mathbf{q}(\alpha_\varphi, \alpha_\vartheta, t) = \mathbf{0}$ and using the method of variable separation, it is possible to seek solutions that are harmonic in time and whose frequency is ω; then, the displacements and the rotations can be written as follows:

$$\begin{aligned}
u_\varphi(\alpha_\varphi, \alpha_\vartheta, t) &= U^\varphi(\alpha_\varphi, \alpha_\vartheta)\mathrm{e}^{\mathrm{i}\omega t} \\
u_\vartheta(\alpha_\varphi, \alpha_\vartheta, t) &= U^\vartheta(\alpha_\varphi, \alpha_\vartheta)\mathrm{e}^{\mathrm{i}\omega t} \\
w(\alpha_\varphi, \alpha_\vartheta, t) &= W^\zeta(\alpha_\varphi, \alpha_\vartheta)\mathrm{e}^{\mathrm{i}\omega t} \\
\beta_\varphi(\alpha_\varphi, \alpha_\vartheta, t) &= B^\varphi(\alpha_\varphi, \alpha_\vartheta)\mathrm{e}^{\mathrm{i}\omega t} \\
\beta_\vartheta(\alpha_\varphi, \alpha_\vartheta, t) &= B^\vartheta(\alpha_\varphi, \alpha_\vartheta)\mathrm{e}^{\mathrm{i}\omega t}
\end{aligned} \tag{4.1}$$

where the vibration spatial amplitude values $(U^\varphi(\alpha_\varphi, \alpha_\vartheta), U^\vartheta(\alpha_\varphi, \alpha_\vartheta), W^\zeta(\alpha_\varphi, \alpha_\vartheta), B^\varphi(\alpha_\varphi, \alpha_\vartheta), B^\vartheta(\alpha_\varphi, \alpha_\vartheta))$ fulfil the fundamental differential system.

The basic steps in the GDQ solution of the free vibration problem of hemispherical dome type structures are as in the following:

- Discretization of independent variables $\varphi \in]0, 90°]$, $\vartheta \in [0, \vartheta_0]$ (with $\vartheta_0 \leq 2\pi$).
- The spatial derivatives are approximated according to GDQ rule.
- The differential governing systems (2.23)–(2.27) are transformed into linear eigenvalue problems for the natural frequencies. The boundary conditions are imposed in the sampling points corresponding to the boundary. All these relations are imposed pointwise.
- The solution of the previously stated discrete system in terms of natural frequencies and mode shape components is worked out. For each mode, local values of dependent variables are used to obtain the complete assessment of the deformed configuration.

4.1. Discretization of motion equations

The simple numerical operations illustrated here, by applying the GDQ procedure, enable one to write the equations of motion in discrete form, transforming each space derivative into a weighted sum of node values of dependent variables. Each of the approximated equations is valid in a single sampling point. The governing equations (2.23)–(2.27) can be discretized as:

$$\begin{aligned}
&\frac{K}{R^2}\sum_{k=1}^{N}\varsigma_{ik}^{\varphi(2)}U_{kj}^{\varphi} + \frac{(1-\nu)}{2}\frac{K}{R_{0i}^2}\sum_{m=1}^{M}\varsigma_{jm}^{\vartheta(2)}U_{mj}^{\varphi} \\
&\quad + \frac{(1+\nu)}{2}\frac{K}{RR_{0i}}\sum_{k=1}^{N}\varsigma_{ik}^{\varphi(1)}\left(\sum_{m=1}^{M}\varsigma_{jm}^{\vartheta(1)}U_{km}^{\vartheta}\right) + K\frac{\cos\varphi_i}{RR_{0i}}\sum_{k=1}^{N}\varsigma_{ik}^{\varphi(1)}U_{kj}^{\varphi} \\
&\quad + \frac{K}{R}\left[\frac{1}{R}\left(1+\frac{(1-\nu)}{2\chi}\right) + \frac{\nu\sin\varphi_i}{R_{0i}}\right]\sum_{k=1}^{N}\varsigma_{ik}^{\varphi(1)}W_{kj}^{\zeta} - K\frac{(3-\nu)}{2}\frac{\cos\varphi_i}{R_{0i}^2}\sum_{m=1}^{M}\varsigma_{jm}^{\vartheta(1)}U_{im}^{\vartheta} \\
&\quad - K\left[\frac{1}{R_{0i}}\left(\frac{\nu\sin\varphi_i}{R} + \frac{\cos^2\varphi_i}{R_{0i}}\right) + \frac{1}{R^2}\frac{(1-\nu)}{2\chi}\right]U_{ij}^{\varphi} + K\frac{\cos\varphi_i}{R_{0i}}\left(\frac{1}{R} - \frac{\sin\varphi_i}{R_{0i}}\right)W_{ij}^{\zeta} \\
&\quad + \frac{(1-\nu)}{2\chi}\frac{K}{R}B_{ij}^{\varphi} = -\omega^2\mu h\left(1+\frac{h^2}{12R^2}\right)U_{ij}^{\varphi} - \omega^2\frac{\mu h^3}{6R}B_{ij}^{\varphi} \\
&\frac{(1-\nu)}{2}\frac{K}{R^2}\sum_{k=1}^{N}\varsigma_{ik}^{\varphi(2)}U_{kj}^{\vartheta} + \frac{K}{R_{0i}^2}\sum_{m=1}^{M}\varsigma_{jm}^{\vartheta(2)}U_{im}^{\vartheta} + \frac{(1+\nu)}{2}\frac{K}{RR_{0i}}\sum_{k=1}^{N}\varsigma_{ik}^{\varphi(1)}\left(\sum_{m=1}^{M}\varsigma_{jm}^{\vartheta(1)}U_{km}^{\varphi}\right) \\
&\quad + K\frac{(1-\nu)}{2}\frac{\cos\varphi_i}{RR_{0i}}\sum_{k=1}^{N}\varsigma_{ik}^{\varphi(1)}U_{kj}^{\vartheta} + K\frac{(3-\nu)}{2}\frac{\cos\varphi_i}{R_{0i}^2}\sum_{m=1}^{M}\varsigma_{jm}^{\vartheta(1)}U_{im}^{\varphi}
\end{aligned} \tag{4.2}$$

$$+\frac{K}{R_{0i}}\left[\frac{\nu}{R}+\frac{\sin\varphi_i}{R_{0i}}\left(1+\frac{(1-\nu)}{2\chi}\right)\right]\sum_{m=1}^{M}\varsigma_{jm}^{\vartheta(1)}W_{im}^{\zeta}+K\frac{(1-\nu)}{2\chi}\frac{\sin\varphi_i}{R_{0i}}B_{ij}^{\vartheta}$$
$$+\frac{(1-\nu)}{2}\frac{K}{R_{0i}}\left[\frac{\sin\varphi_i}{R}-\frac{1}{R_{0i}}\left(\cos^2\varphi_i+\frac{\sin^2\varphi_i}{\chi}\right)\right]U_{ij}^{\vartheta}=-\omega^2\mu h\left(1+\frac{h^2}{12R^2}\right)U_{ij}^{\vartheta}-\omega^2\frac{\mu h^3}{6R}B_{ij}^{\vartheta} \tag{4.3}$$

$$\frac{(1-\nu)}{2\chi}\frac{K}{R^2}\sum_{k=1}^{N}\varsigma_{ik}^{\varphi(2)}W_{kj}^{\zeta}+\frac{(1-\nu)}{2\chi}\frac{K}{R_{0i}^2}\sum_{m=1}^{M}\varsigma_{jm}^{\vartheta(2)}W_{im}^{\zeta}$$
$$-\frac{K}{R}\left[\frac{1}{R}\left(1+\frac{(1-\nu)}{2\chi}\right)+\frac{\nu\sin\varphi_i}{R_{0i}}\right]\sum_{k=1}^{N}\varsigma_{ik}^{\varphi(1)}U_{kj}^{\varphi}$$
$$+K\frac{(1-\nu)}{2\chi}\frac{\cos\varphi_i}{RR_{0i}}\sum_{k=1}^{N}\varsigma_{ik}^{\varphi(1)}W_{kj}^{\zeta}+\frac{(1-\nu)}{2\chi}\frac{K}{R}\sum_{k=1}^{N}\varsigma_{ik}^{\varphi(1)}B_{kj}^{\varphi}$$
$$-\frac{K}{R_{0i}}\left[\frac{\nu}{R}+\frac{\sin\varphi_i}{R_{0i}}\left(1+\frac{(1-\nu)}{2\chi}\right)\right]\sum_{m=1}^{M}\varsigma_{jm}^{\vartheta(1)}U_{im}^{\vartheta}$$
$$+\frac{(1-\nu)}{2\chi}\frac{K}{R_{0i}}\sum_{m=1}^{M}\varsigma_{jm}^{\vartheta(1)}B_{im}^{\vartheta}-K\frac{\cos\varphi_i}{R_{0i}}\left[\frac{\sin\varphi_i}{R_{0i}}+\frac{1}{R}\left(\nu+\frac{(1-\nu)}{2\chi}\right)\right]U_{ij}^{\varphi}$$
$$-K\left[\frac{1}{R}\left(\frac{1}{R}+\frac{2\nu\sin\varphi_i}{R_{0i}}\right)+\frac{\sin^2\varphi_i}{R_{0i}^2}\right]W_{ij}^{\zeta}+K\frac{(1-\nu)}{2\chi}\frac{\cos\varphi_i}{R_{0i}}B_{ij}^{\varphi}=-\omega^2\mu h\left(1+\frac{h^2}{12R^2}\right)W_{ij}^{\zeta} \tag{4.4}$$

$$\frac{D}{R^2}\sum_{k=1}^{N}\varsigma_{ik}^{\varphi(2)}B_{kj}^{\varphi}+\frac{(1-\nu)}{2}\frac{D}{R_{0i}^2}\sum_{m=1}^{M}\varsigma_{jm}^{\vartheta(2)}B_{im}^{\varphi}+\frac{(1+\nu)}{2}\frac{D}{RR_{0i}}\sum_{k=1}^{N}\varsigma_{ik}^{\varphi(1)}\left(\sum_{m=1}^{M}\varsigma_{jm}^{\vartheta(1)}B_{km}^{\vartheta}\right)$$
$$-\frac{(1-\nu)}{2\chi}\frac{K}{R}\sum_{k=1}^{N}\varsigma_{ik}^{\varphi(1)}W_{kj}^{\zeta}+D\frac{\cos\varphi_i}{RR_{0i}}\sum_{k=1}^{N}\varsigma_{ik}^{\varphi(1)}B_{kj}^{\varphi}-D\frac{(3-\nu)}{2}\frac{\cos\varphi_i}{R_{0i}^2}\sum_{m=1}^{M}\varsigma_{jm}^{\vartheta(1)}B_{im}^{\vartheta}$$
$$+\frac{(1-\nu)}{2\chi}\frac{K}{R}U_{ij}^{\varphi}-\left[\frac{D}{R_{0i}}\left(\frac{\nu\sin\varphi_i}{R}+\frac{\cos^2\varphi_i}{R_{0i}}\right)+K\frac{(1-\nu)}{2\chi}\right]B_{ij}^{\varphi}$$
$$=-\omega^2\frac{\mu h^3}{6R}U_{ij}^{\varphi}-\omega^2\mu h^3\left(\frac{1}{12}+\frac{h^2}{80R^2}\right)B_{ij}^{\varphi} \tag{4.5}$$

$$\frac{(1-\nu)}{2}\frac{D}{R^2}\sum_{k=1}^{N}\varsigma_{ik}^{\varphi(2)}B_{kj}^{\vartheta}+\frac{D}{R_{0i}^2}\sum_{m=1}^{M}\varsigma_{jm}^{\vartheta(2)}B_{im}^{\vartheta}+\frac{(1+\nu)}{2}\frac{D}{RR_{0i}}\sum_{k=1}^{N}\varsigma_{ik}^{\varphi(1)}\left(\sum_{m=1}^{M}\varsigma_{jm}^{\vartheta(1)}B_{km}^{\varphi}\right)$$
$$+D\frac{(1-\nu)}{2}\frac{\cos\varphi_i}{RR_{0i}}\sum_{k=1}^{N}\varsigma_{ik}^{\varphi(1)}B_{kj}^{\vartheta}-\frac{(1-\nu)}{2\chi}\frac{K}{R_{0i}}\sum_{m=1}^{M}\varsigma_{jm}^{\vartheta(1)}W_{im}^{\zeta}+D\frac{(3-\nu)}{2}\frac{\cos\varphi_i}{R_{0i}^2}\sum_{m=1}^{M}\varsigma_{jm}^{\vartheta(1)}B_{im}^{\varphi}$$
$$+K\frac{(1-\nu)}{2\chi}\frac{\sin\varphi_i}{R_{0i}}U_{ij}^{\vartheta}+\left[\frac{(1-\nu)}{2}\frac{D}{R_{0i}}\left(\frac{\sin\varphi_i}{R}-\frac{\cos^2\varphi_i}{R_{0i}}\right)-K\frac{(1-\nu)}{2\chi}\right]B_{ij}^{\vartheta}$$
$$=-\omega^2\frac{\mu h^3}{6R}U_{ij}^{\vartheta}-\omega^2\mu h^3\left(\frac{1}{12}+\frac{h^2}{80R^2}\right)B_{ij}^{\vartheta} \tag{4.6}$$

where $i=2,3,\ldots,N-1$, $j=2,3,\ldots,M-1$ and $\varsigma_{ik}^{\varphi(1)}$, $\varsigma_{jm}^{\vartheta(1)}$, $\varsigma_{ik}^{\varphi(2)}$ and $\varsigma_{jm}^{\vartheta(2)}$ are the weighting coefficients of the first and second derivatives in φ and ϑ directions, respectively. N and M are the total number of grid points in φ and ϑ directions.

4.2. Implementation of boundary and compatibility conditions

Applying the GDQ methodology, the discretized forms of the boundary conditions are given as follows:

Clamped edge boundary condition (C):

$$\begin{aligned} &U_{aj}^{\varphi} = U_{aj}^{\vartheta} = W_{aj}^{\zeta} = B_{aj}^{\varphi} = B_{aj}^{\vartheta} = 0 \quad \text{for } a = 1, N \text{ and } j = 1, 2, \ldots, M \\ &U_{ib}^{\varphi} = U_{ib}^{\vartheta} = W_{ib}^{\zeta} = B_{ib}^{\varphi} = B_{ib}^{\vartheta} = 0 \quad \text{for } b = 1, M \text{ and } i = 1, 2, \ldots, N. \end{aligned} \tag{4.7}$$

Simply supported edge boundary condition (S):

$$\begin{cases} U_{aj}^{\varphi} = U_{aj}^{\vartheta} = W_{aj}^{\zeta} = B_{aj}^{\vartheta} = 0 \\ \dfrac{1}{R}\displaystyle\sum_{k=1}^{N} \varsigma_{ak}^{\varphi(1)} B_{kj}^{\varphi} + \frac{\nu}{R_{0a}}\left(\sum_{m=1}^{M} \varsigma_{jm}^{\vartheta(1)} B_{am}^{\vartheta} + B_{aj}^{\varphi}\cos\varphi_a\right) = 0 \end{cases} \quad \text{for } a = 1, N \text{ and } j = 1, 2, \ldots, M$$

$$\begin{cases} U_{ib}^{\varphi} = U_{ib}^{\vartheta} = W_{ib}^{\zeta} = B_{ib}^{\varphi} = 0 \\ \dfrac{1}{R_{0i}}\left(\displaystyle\sum_{m=1}^{M} \varsigma_{bm}^{\vartheta(1)} B_{im}^{\vartheta} + B_{ib}^{\varphi}\cos\varphi_i\right) + \frac{\nu}{R}\sum_{k=1}^{N} \varsigma_{ik}^{\varphi(1)} B_{kb}^{\varphi} = 0 \end{cases} \quad \text{for } b = 1, M \text{ and } i = 1, 2, \ldots, N. \tag{4.8}$$

Free edge boundary condition (F):

$$\begin{cases} \dfrac{1}{R}\left(\displaystyle\sum_{k=1}^{N} \varsigma_{ak}^{\varphi(1)} U_{kj}^{\varphi} + W_{aj}^{\zeta}\right) \\ \quad + \dfrac{\nu}{R_{0a}}\left(\displaystyle\sum_{m=1}^{M} \varsigma_{jm}^{\vartheta(1)} U_{am}^{\vartheta} + U_{aj}^{\varphi}\cos\varphi_a + W_{aj}^{\zeta}\sin\varphi_a\right) = 0 \\ \dfrac{1}{R}\displaystyle\sum_{k=1}^{N} \varsigma_{ak}^{\varphi(1)} U_{kj}^{\vartheta} + \dfrac{1}{R_{0a}}\left(\displaystyle\sum_{m=1}^{M} \varsigma_{jm}^{\vartheta(1)} U_{am}^{\varphi} - U_{aj}^{\vartheta}\cos\varphi_a\right) = 0 \\ \dfrac{1}{R}\left(\displaystyle\sum_{k=1}^{N} \varsigma_{ak}^{\varphi(1)} W_{kj}^{\zeta} - U_{aj}^{\varphi}\right) + B_{aj}^{\varphi} = 0 \\ \dfrac{1}{R}\displaystyle\sum_{k=1}^{N} \varsigma_{ak}^{\varphi(1)} B_{kj}^{\varphi} + \dfrac{\nu}{R_{0a}}\left(\displaystyle\sum_{m=1}^{M} \varsigma_{jm}^{\vartheta(1)} B_{am}^{\vartheta} + B_{aj}^{\varphi}\cos\varphi_a\right) = 0 \\ \dfrac{1}{R}\displaystyle\sum_{k=1}^{N} \varsigma_{ak}^{\varphi(1)} B_{kj}^{\vartheta} + \dfrac{1}{R_{0a}}\left(\displaystyle\sum_{m=1}^{M} \varsigma_{jm}^{\vartheta(1)} B_{am}^{\varphi} - B_{aj}^{\vartheta}\cos\varphi_a\right) = 0 \end{cases} \quad \text{for } a = 1, N \text{ and } j = 1, 2, \ldots, M \tag{4.9}$$

$$\begin{cases} \dfrac{1}{R_{0i}}\left(\displaystyle\sum_{m=1}^{M} \varsigma_{bm}^{\vartheta(1)} U_{im}^{\vartheta} + U_{ib}^{\varphi}\cos\varphi_i + W_{ib}^{\zeta}\sin\varphi_i\right) \\ \quad + \dfrac{\nu}{R}\left(\displaystyle\sum_{k=1}^{N} \varsigma_{ik}^{\varphi(1)} U_{kb}^{\varphi} + W_{ib}^{\zeta}\right) = 0 \\ \dfrac{1}{R}\displaystyle\sum_{k=1}^{N} \varsigma_{ik}^{\varphi(1)} U_{kb}^{\vartheta} + \dfrac{1}{R_{0i}}\left(\displaystyle\sum_{m=1}^{M} \varsigma_{bm}^{\vartheta(1)} U_{im}^{\varphi} - U_{ib}^{\vartheta}\cos\varphi_i\right) = 0 \\ \dfrac{1}{R_{0i}}\left(\displaystyle\sum_{m=1}^{M} \varsigma_{bm}^{\vartheta(1)} W_{im}^{\zeta} - U_{ib}^{\vartheta}\sin\varphi_i\right) + B_{ib}^{\vartheta} = 0 \\ \dfrac{1}{R_{0i}}\left(\displaystyle\sum_{m=1}^{M} \varsigma_{bm}^{\vartheta(1)} B_{im}^{\vartheta} + B_{ib}^{\varphi}\cos\varphi_i\right) + \dfrac{\nu}{R}\displaystyle\sum_{k=1}^{N} \varsigma_{ik}^{\varphi(1)} B_{kb}^{\varphi} = 0 \\ \dfrac{1}{R}\displaystyle\sum_{m=1}^{M} \varsigma_{bm}^{\varphi(1)} B_{im}^{\vartheta} + \dfrac{1}{R_{0i}}\left(\displaystyle\sum_{k=1}^{N} \varsigma_{ik}^{\vartheta(1)} B_{kb}^{\varphi} - B_{ib}^{\vartheta}\cos\varphi_i\right) = 0 \end{cases} \quad \text{for } b = 1, M \text{ and } i = 1, 2, \ldots, N. \tag{4.10}$$

Kinematical and physical compatibility conditions:

$$U_{i1}^{\varphi} = U_{iM}^{\varphi}, \qquad U_{i1}^{\vartheta} = U_{iM}^{\vartheta}, \qquad W_{i1}^{\zeta} = W_{iM}^{\zeta}, \qquad B_{i1}^{\varphi} = B_{iM}^{\varphi}, \qquad B_{i1}^{\vartheta} = B_{iM}^{\vartheta}$$

$$
\begin{cases}
\dfrac{1}{R_{0i}}\left(\displaystyle\sum_{m=1}^{M} \varsigma_{1m}^{\vartheta(1)} U_{im}^{\vartheta} + U_{i1}^{\varphi}\cos\varphi_i + W_{i1}^{\zeta}\sin\varphi_i\right) + \dfrac{\nu}{R}\left(\displaystyle\sum_{k=1}^{N} \varsigma_{ik}^{\varphi(1)} U_{k1}^{\varphi} + W_{i1}^{\zeta}\right) \\
\quad = \dfrac{1}{R_{0i}}\left(\displaystyle\sum_{m=1}^{M} \varsigma_{bm}^{\vartheta(1)} U_{im}^{\vartheta} + U_{iM}^{\varphi}\cos\varphi_i + W_{iM}^{\zeta}\sin\varphi_i\right) + \dfrac{\nu}{R}\left(\displaystyle\sum_{k=1}^{N} \varsigma_{ik}^{\varphi(1)} U_{kM}^{\varphi} + W_{iM}^{\zeta}\right) \\
\dfrac{1}{R}\displaystyle\sum_{k=1}^{N} \varsigma_{ik}^{\varphi(1)} U_{k1}^{\vartheta} + \dfrac{1}{R_{0i}}\left(\displaystyle\sum_{m=1}^{M} \varsigma_{1m}^{\vartheta(1)} U_{im}^{\varphi} - U_{i1}^{\vartheta}\cos\varphi_i\right) \\
\quad = \dfrac{1}{R}\displaystyle\sum_{k=1}^{N} \varsigma_{ik}^{\varphi(1)} U_{kM}^{\vartheta} + \dfrac{1}{R_{0i}}\left(\displaystyle\sum_{m=1}^{M} \varsigma_{Mm}^{\vartheta(1)} U_{im}^{\varphi} - U_{iM}^{\vartheta}\cos\varphi_i\right) \\
\dfrac{1}{R_{0i}}\left(\displaystyle\sum_{m=1}^{M} \varsigma_{1m}^{\vartheta(1)} W_{im}^{\zeta} - U_{i1}^{\vartheta}\sin\varphi_i\right) + B_{i1}^{\vartheta} = \dfrac{1}{R_{0i}}\left(\displaystyle\sum_{m=1}^{M} \varsigma_{Mm}^{\vartheta(1)} W_{im}^{\zeta} - U_{iM}^{\vartheta}\sin\varphi_i\right) + B_{iM}^{\vartheta} \\
\dfrac{1}{R_{0i}}\left(\displaystyle\sum_{m=1}^{M} \varsigma_{1m}^{\vartheta(1)} B_{im}^{\vartheta} + B_{i1}^{\varphi}\cos\varphi_i\right) + \dfrac{\nu}{R}\displaystyle\sum_{k=1}^{N} \varsigma_{ik}^{\varphi(1)} B_{k1}^{\varphi} \\
\quad = \dfrac{1}{R_{0i}}\left(\displaystyle\sum_{m=1}^{M} \varsigma_{Mm}^{\vartheta(1)} B_{im}^{\vartheta} + B_{iM}^{\varphi}\cos\varphi_i\right) + \dfrac{\nu}{R}\displaystyle\sum_{k=1}^{N} \varsigma_{ik}^{\varphi(1)} B_{kM}^{\varphi} \\
\dfrac{1}{R}\displaystyle\sum_{m=1}^{M} \varsigma_{1m}^{\varphi(1)} B_{im}^{\vartheta} + \dfrac{1}{R_{0i}}\left(\displaystyle\sum_{k=1}^{N} \varsigma_{ik}^{\vartheta(1)} B_{k1}^{\varphi} - B_{i1}^{\vartheta}\cos\varphi_i\right) \\
\quad = \dfrac{1}{R}\displaystyle\sum_{m=1}^{M} \varsigma_{Mm}^{\varphi(1)} B_{im}^{\vartheta} + \dfrac{1}{R_{0i}}\left(\displaystyle\sum_{k=1}^{N} \varsigma_{ik}^{\vartheta(1)} B_{kM}^{\varphi} - B_{iM}^{\vartheta}\cos\varphi_i\right) \quad \text{for } i = 2, \ldots, N-1.
\end{cases}
\tag{4.11}
$$

4.3. Solution procedure

Applying the differential quadrature procedure, the whole system of differential equations has been discretized and the global assembling leads to the following set of linear algebraic equations:

$$
\left[\begin{array}{c|c} \mathbf{K}_{bb} & \mathbf{K}_{bd} \\ \hline \mathbf{K}_{db} & \mathbf{K}_{dd} \end{array}\right]\left[\begin{array}{c} \boldsymbol{\delta}_b \\ \hline \boldsymbol{\delta}_d \end{array}\right] = \omega^2 \left[\begin{array}{c|c} \mathbf{0} & \mathbf{0} \\ \hline \mathbf{0} & \mathbf{M}_{dd} \end{array}\right]\left[\begin{array}{c} \boldsymbol{\delta}_b \\ \hline \boldsymbol{\delta}_d \end{array}\right]. \tag{4.12}
$$

In the above matrices and vectors, the partitioning is set forth by subscripts b and d, referring to the system degrees of freedom and standing for boundary and domain, respectively. In order to make the computation more efficient, kinematic condensation of non-domain degrees of freedom is performed:

$$
(\mathbf{K}_{dd} - \mathbf{K}_{db}(\mathbf{K}_{bb})^{-1}\mathbf{K}_{bd})\boldsymbol{\delta}_d = \omega^2 \mathbf{M}_{dd}\boldsymbol{\delta}_d. \tag{4.13}
$$

The natural frequencies of the structure considered can be determined by making the following determinant vanish:

$$
\left|(\mathbf{K}_{dd} - \mathbf{K}_{db}(\mathbf{K}_{bb})^{-1}\mathbf{K}_{bd}) - \omega^2 \mathbf{M}_{dd}\right| = 0. \tag{4.14}
$$

5. Numerical applications and discussion

Based on the above derivations, in the present paragraph some results and considerations about the free vibration problem of hemispherical panels and hemispherical domes are presented. The analysis has been carried out by means of numerical procedures illustrated above. The mechanical characteristics for the considered structures are listed in Table 1. In order to verify the accuracy of the present method, some comparisons have also been performed. The first ten natural frequencies of a hemispherical panel and a hemispherical dome are reported in Tables 2–7. The details regarding the geometry of the considered structures are indicated below:

– *Hemispherical panel*: $R = 1$ m, $h = 0.1$ m, $\varphi_0 = 30°$, $\varphi_1 = 90°$, $\vartheta_0 = 120°$ (Tables 2–4).
– *Hemispherical dome*: $R = 1$ m, $h = 0.1$ m, $\varphi_0 = 30°$, $\varphi_1 = 90°$, $\vartheta_0 = 360°$ (Tables 5–7).

Table 1
Physical parameters used in the analysis of free vibrations of the structures considered

Parameter	Value
Density of mass μ	7800 kg/m^3
Young's modulus E	2.1×10^{11} Pa
Poisson coefficient ν	0.3
Shear factor χ	6/5

Table 2
Shell theory for the hemispherical panel C–C–F–F

Frequencies (Hz)	GDQ method	Abaqus	Ansys	Femap\Nastran	Straus	Pro\Engineer
f_1	327.00	326.94	328.48	328.69	327.28	327.39
f_2	458.79	459.01	460.89	460.93	458.54	458.58
f_3	706.37	706.98	710.52	711.09	706.64	705.71
f_4	885.00	884.09	893.51	892.71	888.86	885.18
f_5	1047.57	1047.62	1056.12	1055.81	1049.49	1046.55
f_6	1272.59	1270.77	1285.21	1282.41	1278.91	1270.72
f_7	1304.62	1309.19	1327.96	1325.89	1313.90	1305.12
f_8	1383.57	1383.72	1403.99	1401.91	1395.46	1382.81
f_9	1442.29	1444.59	1458.62	1455.97	1451.84	1443.60
f_{10}	1597.92	1602.13	1622.34	1619.97	1610.04	1600.55

Table 3
3D element theory for the hemispherical panel C–C–F–F

Frequencies (Hz)	Abaqus	Ansys	Femap\Nastran	Straus	Pro\Engineer
f_1	328.09	328.09	327.91	327.85	328.78
f_2	460.28	460.27	459.91	459.78	461.33
f_3	707.53	707.53	706.88	706.66	709.03
f_4	886.50	886.50	885.39	884.94	887.82
f_5	1048.18	1048.18	1047.07	1046.63	1050.78
f_6	1273.43	1273.44	1271.89	1271.26	1276.11
f_7	1308.84	1308.87	1305.45	1304.21	1314.80
f_8	1386.88	1386.85	1384.38	1383.53	1392.22
f_9	1443.57	1443.57	1441.70	1440.89	1447.00
f_{10}	1603.23	1603.23	1599.70	1598.32	1610.11

Table 4
Shell theory for the hemispherical panel S–S–F–F

Frequencies (Hz)	f_1	f_2	f_3	f_4	f_5
GDQ Method	298.44	395.78	657.29	818.19	962.15
Abaqus	297.94	396.18	656.34	816.48	961.61
Ansys	299.66	397.80	660.45	825.65	969.55
Femap\Nastran	299.62	396.98	660.88	824.84	967.84
Straus	299.28	397.42	659.35	824.22	968.35
Pro\Engineer WF	298.72	395.79	656.66	818.56	961.26

The geometrical boundary conditions for the hemispherical panel are identified by the following convention. For example, the symbolism C–S–C–F indicates that the edges $\varphi = \varphi_1$, $\vartheta = \vartheta_0$, $\varphi = \varphi_0$, $\vartheta = 0$ are clamped, simply supported, clamped and free, respectively. In particular, we have considered the hemispherical panels characterized by C–C–F–F and S–S–F–F boundary conditions (Tables 2–4). For the hemispherical dome, for example, the symbolism C–F indicates that the edges $\varphi = \varphi_1$ and $\varphi = \varphi_0$ are clamped and free, respectively. In this case, the missing boundary conditions are the kinematical and physical compatibility conditions that are applied at the same meridian for $\vartheta = 0$

Table 5
Shell theory for the hemispherical dome C–F

Frequencies (Hz)	GDQ Method	Abaqus	Ansys	Femap\Nastran	Straus	Pro\Engineer
f_1	369.34	369.41	370.19	370.43	369.64	369.33
f_2	369.34	369.41	370.19	370.43	369.71	369.33
f_3	581.91	584.05	582.43	582.68	582.08	582.16
f_4	581.91	584.05	582.43	582.68	582.12	582.16
f_5	628.57	625.65	631.64	632.01	628.43	628.16
f_6	628.57	625.65	631.64	632.01	628.45	628.16
f_7	811.07	811.17	814.28	813.34	811.54	809.59
f_8	888.98	888.83	893.55	893.25	889.42	887.69
f_9	888.98	888.83	893.56	893.25	889.86	887.69
f_{10}	965.75	964.17	973.15	971.75	967.55	964.64

Table 6
3D element theory for the hemispherical dome C–F

Frequencies (Hz)	Abaqus	Ansys	Femap\Nastran	Straus	Pro\Engineer
f_1	369.99	369.76	369.80	370.22	370.46
f_2	369.99	369.76	369.80	370.26	370.50
f_3	582.04	582.06	581.93	582.28	582.30
f_4	582.02	582.06	581.93	582.31	582.49
f_5	630.74	629.27	630.22	630.00	630.55
f_6	630.74	629.27	630.22	630.05	630.69
f_7	811.65	811.64	810.54	810.87	812.65
f_8	889.26	889.14	887.94	888.27	890.60
f_9	889.26	889.14	887.94	888.27	890.80
f_{10}	967.29	965.48	966.23	966.17	967.92

Table 7
Shell theory for the hemispherical dome S–F

Frequencies (Hz)	f_1	f_2	f_3	f_4	f_5
GDQ Method	339.78	339.78	544.35	544.35	615.68
Abaqus	338.44	338.44	545.16	545.16	611.06
Ansys	340.51	340.53	544.88	544.88	618.56
Femap\Nastran	340.71	340.71	545.17	545.17	618.75
Straus	340.17	340.22	544.73	544.82	616.91
Pro\Engineer WF	339.78	339.78	544.56	544.56	615.28

and $\vartheta = 2\pi$. In this work the hemispherical dome that we have examined is characterized by C–F and S–F boundary conditions (Tables 5–7).

One of the aims of this paper is to compare results from the present analysis with those obtained by finite element techniques and based on the same shell theory or 3D element theory. In Tables 2, 4, 5 and 7, we have compared the 2D shell theory results obtained by the GDQ Method with the FEM results obtained by some commercial programs using the same 2D shell theory. On the other hand, the FEM solutions using 3D element theory obtained with the same commercial programs are reported in Tables 3 and 6.

For the GDQ results reported in Tables 2, 4, 5 and 7, we have considered the grid distribution with $N = 21$ and $M = 21$. For the commercial programs, we have used shell elements with 8 nodes in Tables 2, 4, 5 and 7. On the other hand, brick-elements with 20-nodes were used for the 3D element theory in Tables 3 and 6.

It is noteworthy that the results from the present methodology are very close to those obtained by the commercial programs. As can be seen, the numerical results show excellent agreement. Furthermore, it is significant that the computational effort in terms of time and number of grid points is smaller for the GDQ method results than for the finite element method.

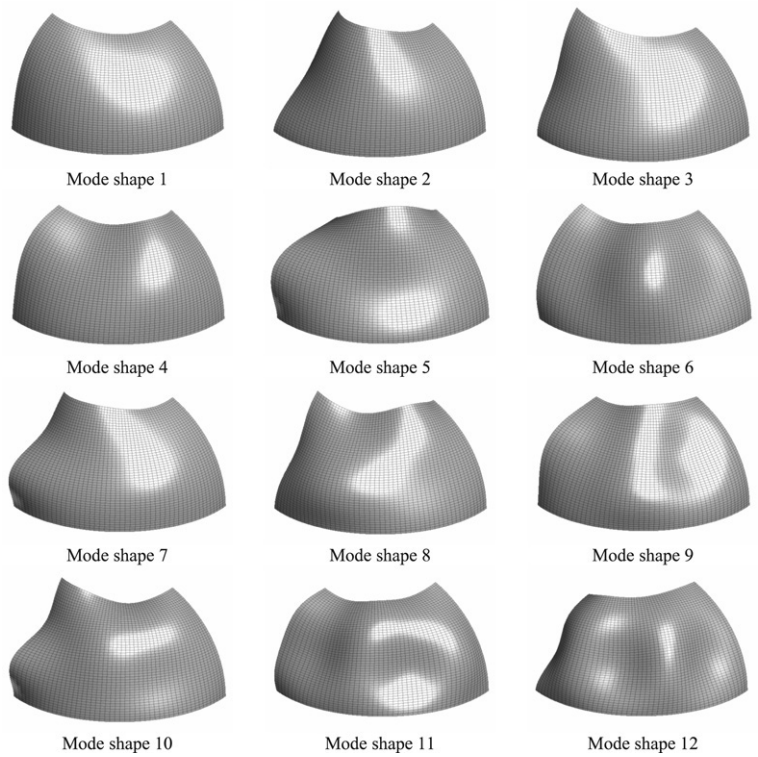

Fig. 6. Mode shapes for the hemispherical panel C–C–F–F.

In Fig. 6, we have reported the first mode shapes for the hemispherical panel characterized by C–C–F–F boundary conditions, while in Fig. 7 the mode shapes for the hemispherical dome characterized by C–F boundary conditions are illustrated. In particular, for the hemispherical dome there are some symmetrical mode shapes due to the symmetry of the problem considered in 3D space. In these cases, we have summarized the symmetrical mode shapes in one figure.

The convergence and the stability of some natural frequencies for the structures under consideration with various grid distributions are shown in Figs. 8–11. Well convergent results for the frequencies can be obtained, if non-uniform grid point distributions are considered. In fact, the uniform grid distribution always presents less accurate results compared to non-uniform grids. It can be seen from the figures that the Chebyshev–Gauss–Lobatto (C–G) grid point distribution has the most rapid converging speed and provides more accurate solutions. Instead, the solutions obtained by using Chebyshev I° (C I°), Chebyshev II° (C II°), Legendre (Leg) and Quadratic (Quad) grid point distributions oscillate much more. It is shown that the solution accuracy of the non-uniform grid distributions stays steady with increasing N and does not decrease due to the numerical instabilities even if N becomes too large. For all the treated cases the non-uniform distributions are stable if the number of grid points increases. As shown in all the figures under consideration, to obtain accurate results for the higher frequencies the number of sampling points must not be too large.

Fig. 8 presents the convergence characteristics of some frequencies for the hemispherical panel characterized by C–C–F–F boundary conditions, while Fig. 9 shows the same characteristics for the hemispherical dome characterized by C–F boundary conditions. The boundary conditions influence the convergence and stability characteristics. In fact, it can be seen from these figures that the solutions for the hemispherical panel have the most rapid converging speed and provide more accurate results with a lower number of sampling points. These cases, when $N = M = 17$, yield very accurate results for the considered frequencies. Instead, the worked solutions for the hemispherical dome oscillate much more and require a larger number of sampling points. In this case, compatibility conditions are introduced and must be implemented to solve the complete shell of revolution problem. To obtain accurate results for the higher frequencies, it is necessary to use a grid distribution with $N = M = 21$ sampling points. In fact, these frequencies show the slower convergence rate.

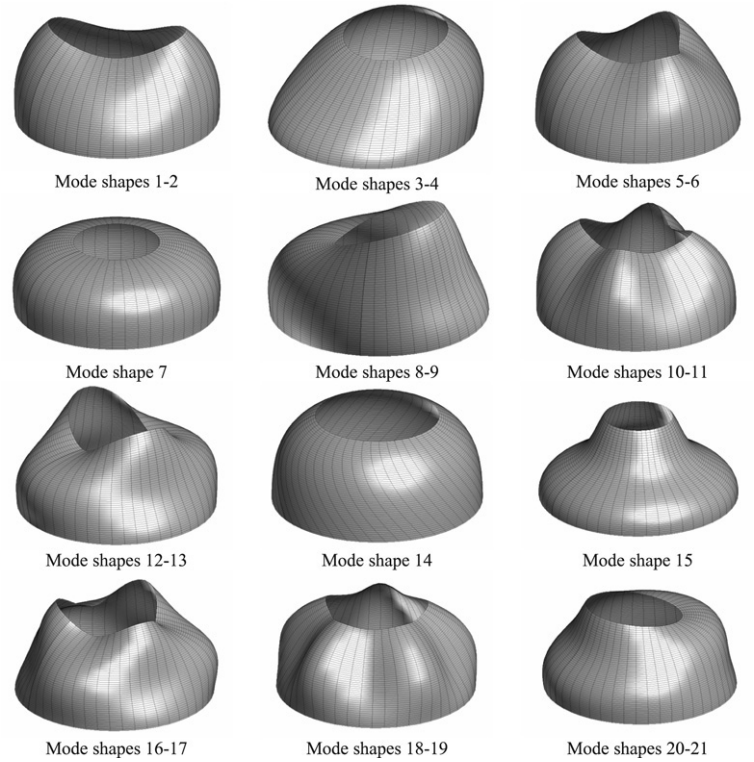

Fig. 7. Mode shapes for the hemispherical dome C–F.

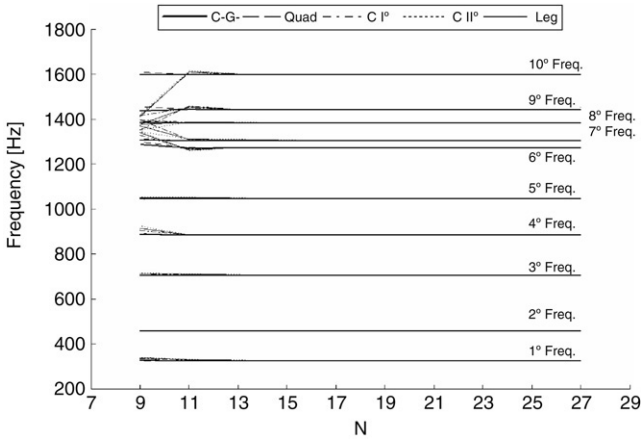

Fig. 8. Convergence and stability characteristics of the first ten frequencies for the hemispherical panel C–C–F–F using different typical grid distributions.

Figs. 10 and 11 show the convergence characteristics of some frequencies for the hemispherical panel and for the hemispherical dome, respectively. The stretch formulation coupled to the Chebyshev–Gauss–Lobatto grid with different stretching parameter β has been used. The same stretching parameter in the φ meridional and ϑ circumferential directions, respectively, is assumed. It is worth noting that, varying the grid spacing by means of different values of β, the GDQ solutions keep the same stability characteristic, while the converging speed and the accuracy depend on the stretching parameter. In particular, there exists an optimal grid point distribution, which corresponds to the optimal stretching parameter and to the optimal polynomial approximation. The GDQ solutions for the hemispherical panel have the most rapid converging speed for each stretching parameter. Instead, the solutions

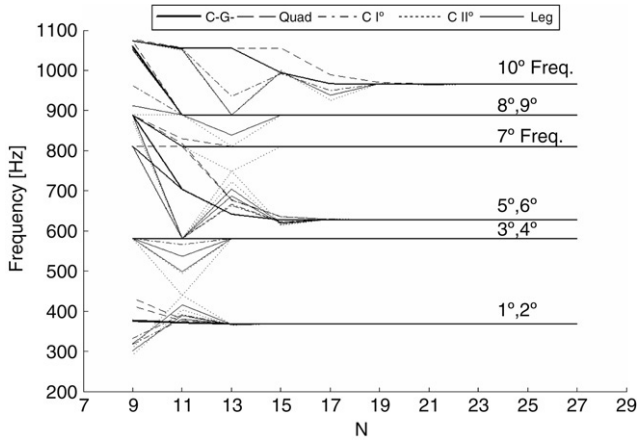

Fig. 9. Convergence and stability characteristics of the first ten frequencies for the hemispherical dome C–F using different typical grid distributions.

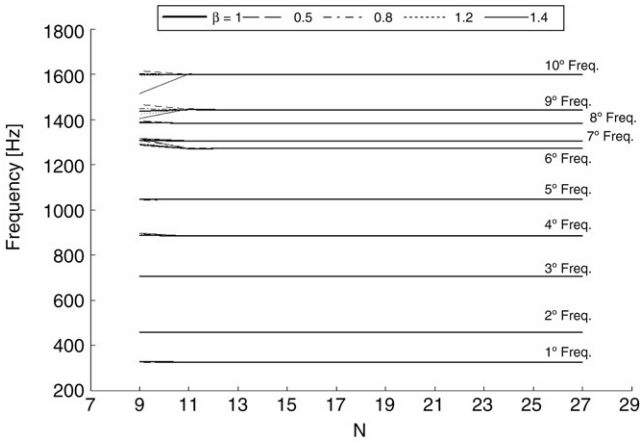

Fig. 10. Convergence and stability characteristics of the first ten frequencies for the hemispherical panel C–C–F–F using the stretch formulation coupled to the Chebyshev–Gauss–Lobatto grid.

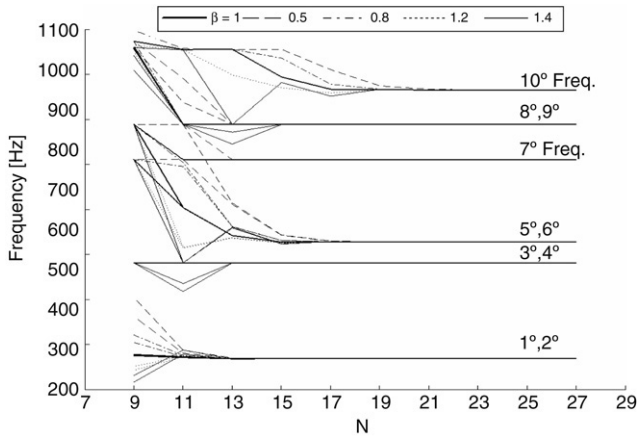

Fig. 11. Convergence and stability characteristics of the first ten frequencies for the hemispherical dome C–F using the stretch formulation coupled to the Chebyshev–Gauss–Lobatto grid.

for the hemispherical dome oscillate much more when the stretching parameter is varied. In particular, the solution improves the converging characteristics using $\beta = 1.2$.

6. Conclusions

A Generalized Differential Quadrature Method application to free vibration analysis of spherical shells has been presented to illustrate the versatility and the accuracy of this methodology. The adopted shell theory is a first-order shear deformation theory. The dynamic equilibrium equations are discretized and solved with the present method giving a standard linear eigenvalue problem. The vibration results are obtained without the modal expansion methodology. The complete 2D differential system, governing the structural problem, has been solved. Due to the theoretical framework, no approximation (δ-point technique) is needed in modelling the boundary edge conditions.

Various boundary conditions and grid point distributions have been considered. The GDQ method provides a very simple algebraic formula for determining the weighting coefficients required by the differential quadrature approximation without restricting in any way the choice of mesh grids. Examples presented show that the generalized differential quadrature method can produce accurate results utilizing only a small number of sampling points. The present method provides convergent results for all the cases as the number of grid points increases. Furthermore, discretizing and programming procedures are quite easy. Fast convergence and very good stability have been shown. The effect of grid point distribution on the GDQ solution of the structural shell problem has been investigated. It was found that the Chebyshev–Gauss–Lobatto grid performs the best among the other four non-uniform typical grid distributions for all cases analyzed. The stretched C–G grid with a proper choice of stretching parameter can improve the convergence characteristics and the accuracy of the numerical solution. Furthermore, it has been shown that the convergence characteristics also depend on the boundary conditions.

Acknowledgments

This research was supported by the Italian Ministry for University and Scientific, Technological Research MIUR (40% and 60%). The research topic is one of the subjects of the Centre of Study and Research for the Identification of Materials and Structures (CIMEST)-"M.Capurso" of the University of Bologna (Italy).

References

[1] J.L. Sanders, An improved first approximation theory of thin shells, NASA Report, 24, 1959.
[2] W. Flügge, Stress in Shells, Springer, New York, 1960.
[3] F.I. Niordson, Shell Theory, North-Holland, Amsterdam, 1985.
[4] E. Reissner, The effect of transverse shear deformation on the bending of elastic plates, J. Appl. Mech. ASME 12 (1945) 66–77.
[5] E. Viola, E. Artioli, The G.D.Q. method for the harmonic dynamic analysis of rotational shell structural elements, Struct. Eng. Mech. 17 (2004) 789–817.
[6] E. Artioli, P. Gould, E. Viola, Generalized collocation method for rotational shells free vibration analysis. in: The Seventh International Conference on Computational Structures Technology, Lisbon Portugal, September 7–9, 2004.
[7] C. Shu, Generalized differential–integral quadrature and application to the simulation of incompressible viscous flows including parallel computation, Ph.D. Thesis, University of Glasgow, 1991.
[8] R. Bellman, J. Casti, Differential quadrature and long-term integration, J. Math. Anal. Appl. 34 (1971) 235–238.
[9] R. Bellman, B.G. Kashef, J. Casti, Differential quadrature: A technique for the rapid solution of nonlinear partial differential equations, J. Comput. Phys. 10 (1972) 40–52.
[10] J.R. Quan, C.T. Chang, New insights in solving distributed system equations by the quadrature method — I. Analysis, Comput. Chem. Eng. 13 (1989) 779–788.
[11] J.R. Quan, C.T. Chang, New insights in solving distributed system equations by the quadrature method — II. Numerical experiments, Comput. Chem. Eng. 13 (1989) 1017–1024.
[12] C.W. Bert, S.K. Jang, A.G. Striz, Two new approximate methods for analyzing free vibration of structural components, AIAA J. 26 (1988) 612–618.
[13] F. Civan, C.M. Sliepcevich, Differential quadrature for multi-dimensional problems, J. Math. Anal. Appl. 101 (1984) 423–443.
[14] F. Civan, C.M. Sliepcevich, Application of differential quadrature in solution of pool boiling in cavities, Proc. Oklahoma Acad. Sci. 65 (1985) 73–78.
[15] S. Jang, C. Bert, A.G. Striz, Application of differential quadrature to static analysis of structural components, Internat. J. Numer. Methods Engrg. 28 (1989) 561–577.
[16] G. Karami, P. Malekzadeh, Application of a new differential quadrature methodology for free vibration analysis of plates, Internat. J. Numer. Methods Engrg. 56 (2003) 847–868.

[17] C. Shu, Differential Quadrature and Its Application in Engineering, Springer, Berlin, 2000.
[18] C. Bert, M. Malik, Differential quadrature method in computational mechanics, Appl. Mech. Rev. 49 (1996) 1–27.
[19] C. Shu, W. Chen, On optimal selection of interior points for applying discretized boundary conditions in DQ vibration analysis of beams and plates, J. Sound Vibration 222 (1999) 239–257.
[20] C. Shu, W. Chen, H. Xue, H. Du, Numerical study of grid distribution effect on accuracy of DQ analysis of beams and plates by error estimation of derivative approximation, Internat. J. Numer. Methods Engrg. 51 (2001) 159–179.